Chapter 12
Extrapolating Dynamic Transfer Functions from Multi-Input Multi-Output Vibration Testing and Simulation

E. J. Perez, E. E. Regula, C. J. Wynn, J. D. Blessinger, J. L. Davis, E. P. Dawson, and S. J. Zimmerman

Abstract Finding transfer functions between an applied force and a measured output is well defined for dynamic systems. These transfer functions, which assume a force input, can have many names depending on the output they measure, such as receptance for displacement, mobility for velocity, or accelerance for acceleration. Similarly, the transfer path is a type of transfer function, which is simply the ratio of two outputs from a system in the frequency domain. For single-input linear systems, finding the transfer path between two outputs is a well-understood calculation. These techniques become more complex when dealing with multi-input multi-output tests. While these multi-input vibration tests are more complicated, they provide a more complete understanding of the system being analyzed. These complex systems have well-defined methods for obtaining transfer functions if a forcing function is known. However, when the input force is not known, the methods to find the transfer path between two locations is less understood. This work explores methods for finding unknown transfer paths using accelerations. The tests and validations are done using the Box Assembly, a common structure used in dynamics testing. Experimentally measured and finite-element approximated transfer functions are used to create a transmissibility matrix. This matrix allows for estimation of unknown accelerations based on measured accelerations at different locations on the box assembly.

Keywords Transfer Paths · Transmissibility · FRF · MIMO · FEA

Introduction

Frequency response functions (FRFs) are well understood in dynamic systems and are useful for system identification and structural health monitoring. Finding the FRF for a single-input single-output (SISO) case is straightforward, as only scalar values are used. However, these calculations become more complex with multi-input multi-output (MIMO) testing because the scalar values are replaced with matrices. Not only are the FRFs of MIMO harder to obtain, but so are the transfer paths. Similar to FRFs, which are ratios of output to input, transfer paths are ratios of two system outputs. This relationship

E. J. Perez
Department of Engineering, University of California Riverside, Riverside, CA 92524
e-mail: epere194@ucr.edu

E. E. Regula
Department of Engineering, Messiah University, Mechanicsburg, PA 17055
e-mail: er1324@messiah.edu

C. J. Wynn
Department of Engineering, University of Utah, Salt Lake City, UT 84112
e-mail: cjwynn7@outlook.com

J. D. Blessinger
Los Alamos National Laboratory, Los Alamos, NM 87545
e-mail: jbless@lanl.gov

S. J. Zimmerman
Department of Engineering, University of Southern Indiana, Evansville, IN 47712
e-mail: edawson@lanl.gov

Walter D'Ambrogio, et al. (eds.), *Dynamic Substructuring & Transfer Path Analysis, Vol. 4*, Conference Proceedings of the Society for Experimental Mechanics Series, https://doi.org/10.13052/97887-438-0149-8_12

defines the movement of one location relative to another for any set forcing scenario. These transfer paths can be placed into a transmissibility matrix that defines the contribution of any output to any other distinct output. These transmissibility matrices are different for all independent forcing scenarios. Using these methods, it may be possible to also find theoretical FRFs from locations that have no input during testing but do have measured accelerations. This has the potential to save test engineers time and money on large tests, allowing them to measure acceleration at multiple points while not having to force at those points, and predicting FRFs from those locations.

The box assembly (BA), which can be seen in Figure 1, was utilized for this research. This subassembly of the box assembly with removable component (BARC) structure is commonly used as a test object in multi-axis dynamic testing. Abaqus CAE was used to model the BA for finite-element analysis (FEA). This software allows for the extraction of mass and stiffness matrices which can then be imported into MATLAB to be used to calculate the FRFs and transfer paths used in modeling.

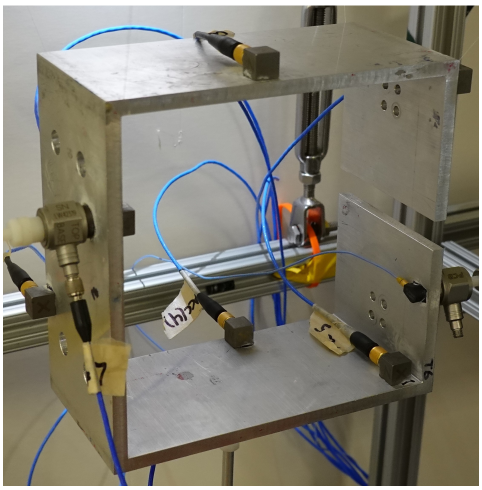

(a) Experimental test setup

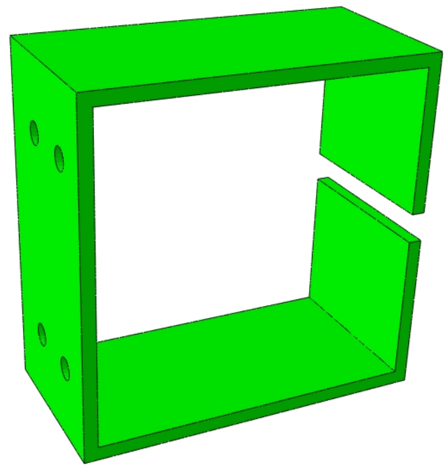

(b) Abaqus model

Fig. 1 Box assembly configuration used in both experimental and numerical approach

The concept of a transfer path has been previously explored as a method of defining the relationships between different points in a MIMO system. The basic expression, as seen in Equation 1, follows previous calculations [1, 2, 3]. Where T is the transfer path while H_u and H_k are the unknown (u) and known (k) frequency response functions of interest.

$$T = \frac{H_u}{H_k} \tag{1}$$

The transfer path in Equation 1 is a scalar one to one relationship, as it is dependent on two single FRFs. Another method of expressing the transfer path between two outputs of a system is to use the pure responses. Using Equations 2 and 3, the response of the system can be obtained, where f_k is the known forcing magnitude of the system and x_u and x_k are responses of the system in the frequency domain. The transfer path from x_u to x_k can be obtained as shown in Equations 2, 3, and 4.

$$x_u = H_u \cdot f_k \tag{2}$$

$$x_k = H_k \cdot f_k \tag{3}$$

$$T = \frac{x_u}{x_k} \tag{4}$$

The transmissibility matrix is then derived from evaluating the transfer path of multiple outputs to multiple outputs at once. If $[H_k]$ is a $n \times n$ matrix and $[H_u]$ is a $m \times n$ matrix, then Equation 5 shows the transmissibility matrix obtained from $[H_u]$ and $[H_k]$.

$$[T] = [H_u][H_k]^{-1} \tag{5}$$

It is important to note that when computing the transmissibility matrix shown in Equation 5, it does not hold the same information as the one to one transfer path obtained with Equation 1. That is to say, the individual elements in the transmissibility matrix are not one to one transfer paths. Rather, an element in the transmissibility matrix is the contribution weighting of a degree of freedom (DOF) from the the set of knowns to a DOF from the set of unknowns. Using similar methods described above, the transmissibility matrix can be computed using a set of unknown and known responses.

$$[x_u] = [\{x_u\}_1\{x_u\}_2 \dots \{x_u\}_n] = [H_u][\{f_k\}_1\{f_k\}_2 \dots \{f_k\}_n] = [H_u][F] \tag{6}$$

$$[x_k] = [\{x_k\}_1\{x_k\}_2 \dots \{x_k\}_n] = [H_k][\{f_k\}_1\{f_k\}_2 \dots \{f_k\}_n] = [H_k][F] \tag{7}$$

$$[T] = [\{x_u\}_1\{x_u\}_2 \dots \{x_u\}_n][\{x_k\}_1\{x_k\}_2 \dots \{x_k\}_n]^{-1} = [x_u][x_k]^{-1} \tag{8}$$

Here, $[x_u]$ and $[x_k]$ are obtained from the known and unknown FRF matrix, $[H]$, as well as the force matrix, $[F]$. Here the force matrix is comprised of multiple forcing vectors as seen in Equations 6 and 7, where each column vector indicates a forcing case. These forcing cases are necessary to expand the size of the $[x_k]$ matrix. Equation 8 is satisfied as long as the number of columns in $[x_u]$ is equal to the number of columns in $[x_k]$, all while $[x_k]$ is maintained a square matrix. Which means the number of forcing cases must be equal to the number of known outputs. This indicates that the size of the forcing matrix is dependent on the number of known outputs and number of forcing locations. To be explicit, the forcing matrix in Equation 7 and 6 is a $m \times n$ matrix where, $m =$ number of forcing locations onto the system and $n =$ number of known outputs. It is also important that the forcing matrix is full ranked to successfully obtain the full contributions within the transmissibility matrix.

However, these processes have some limitations, as the necessary step of inverting the known response of the system requires a square matrix. Maintaining a square matrix while increasing the number of known responses requires an equal increase in the load vector's length. Thus, when increasing the size of the known square matrix, it is also necessary to increase the number of columns of the unknown response matrix to match the size of the square matrix. If the known response matrix to be non-square, a pseudo-inverse operator must be employed.

For example, computing the transmissibility matrix with n known responses with only two load vectors can be illustrated as $[T] = [x_u]_{2\times 2} \cdot [x_k]^{\dagger}_{n\times 2}$. Where $[x_k]^{\dagger}$ is the pseudo-inverse of the non-square matrix $[x_k]$. Even though $[x_k]$ has n rows and two columns, the pseudo-inverse (†) can be used to compute the transmissibility matrix. To verify equivalence, computation of an FRF, $[H_u]_{11}$, was made using the pseudo-inverse operator on a non-square matrix and the traditional inverse for a square matrix. In general, using Equation 5 and the fact that no information is lost calculating $[H_u]_{11}$ from either a square or non-square matrix, then Equation 9 holds.

$$H_u = \sum_{i=1}^{2} T_{1i} \cdot H_{i1k} = \sum_{j=1}^{n} T_{1j} \cdot H_{j1_k} \tag{9}$$

Figure 2 shows the overlay of an FRF ($[H_u]_{11}$) gathered using two different methods, but for the same system. The first method is by using $[H]_k$ of size 2 × 2, while the second uses $[H]_k$ of size 2 × 100. This second method required the use of a pseudo-inverse if no other changes were made to the $[H]_u$ matrix and forcing vectors. In Figure 2, it shows that both methods are equal.

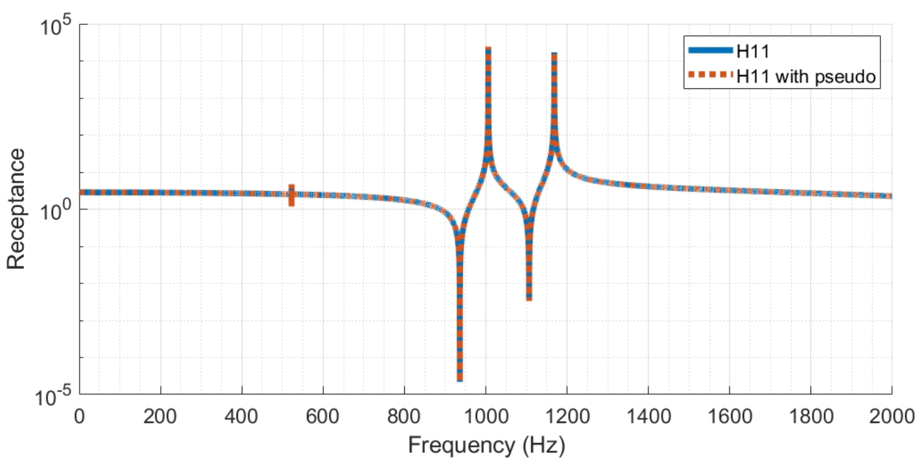

Fig. 2 Receptance calculated with square matrices vs with pseudo inverse.

These methods allow the transmissibility matrix to be calculated with solely experimental data, with solely FEA, or with a combination of the two. For example, if there is a limited number of sensors for experimentation, the acceleration data of one location can be experimentally gathered and FEA can be used to estimate the acceleration of another location. These two sets of data can be used to find a transfer path between the two locations.

The transmissibility matrix may also be acquired in other ways, including construction using the results from Spectral Power Density (SPD) and Singular Value Decomposition (SVD) [4]. Several different methodologies by which the accuracy of the transmissibility matrix may be evaluated using power spectrum density or H-estimators have also been investigated [5, 6].

Many methods of gathering MIMO FRFs and transmissibility matrices require known forcing inputs. This research seeks to establish reliable and accurate methodologies which would allow for FRFs to be estimated between measured accelerations without the need for knowledge about forcing. An added benefit of this approach would be the development of a method by which the forcing can actually be discovered and characterized by measurement of the accelerations at specific points. The benefits of expanding this technique into the realm of MIMO FRFs were also evaluated by their accuracy and efficacy against techniques with similar goals using SISO FRFs.

These techniques were evaluated numerically through simulation as well as experimentally through physical measurement and verification using a BA. The numerical techniques were also used to attempt to predict the unknown FRF matrix seen in the earlier calculations in order to help derive a transmissibility matrix.

Analysis

The BA was analyzed in two different ways, numerically and experimentally. Numerical evaluation of the system was conducted first in order to gather an informed prediction of sensor and shaker placement, as well as an overall idea of the dynamics of the structure. The first step in the numerical evaluation of the BA was the creation of an FEA model and the validation of its accuracy. To achieve this goal, a model based on measurements of the test structure was created, this model was created in Abaqus using C3D8R elements. Once the model was made, a frequency analysis was performed to gather all the natural frequencies under 2000 Hz. This process was repeated several times with slightly different variations of the model. For example, in one model, the bolt holes in the bottom of the structure were modeled, in the other they were left out. Also, different global meshing sizes were used until there was a convergence in the predicted values, as shown in Figure 3. This Figure also shows the time to compute the natural frequencies for the structure, demonstrating the dramatic increase in computation time relative to mesh seed size. The BA is made from Aluminum 6061-T6 and was modeled as such in Abaqus. The model used a density of 2700 kg/m^3, a Young's modulus of 68.9 GPa, and a Poisson's ratio of 0.33.

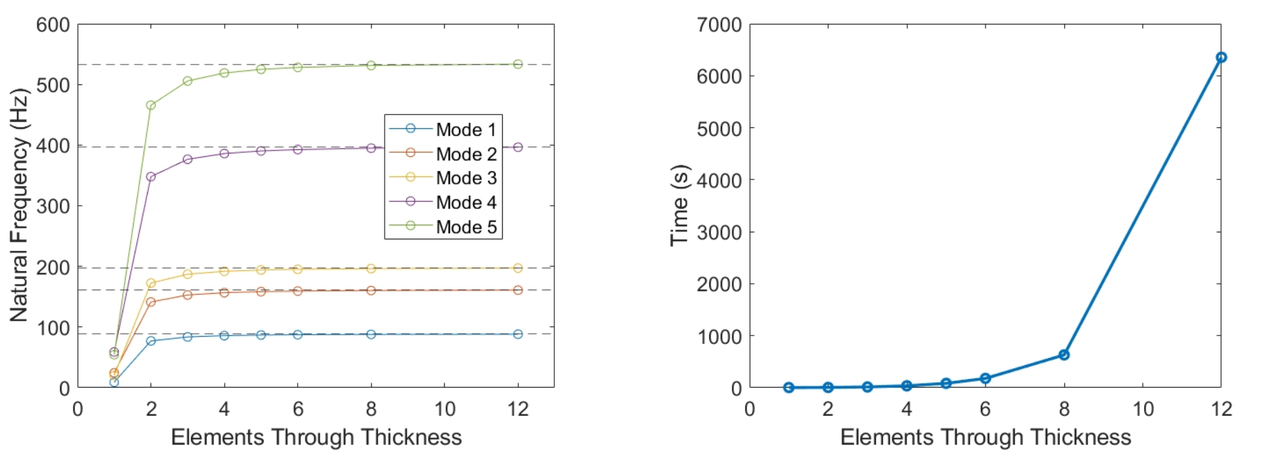

(a) Convergence of natural frequencies for varying mesh seed sizes (b) Time taken for computation to complete based on mesh seed sizes

Fig. 3 Mesh convergence study performed on the numerical BA.

The values of some of the larger mesh sizes were then compared with the smallest size to find a more computationally efficient model that retained most of its accuracy. To do this, percent differences were calculated between the finest mesh size, and the next three smallest mesh sizes. Five elements through the thickness was chosen to model the BA as there was only a

∼1.5% error to the highest fidelity model. Additionally, FEA tests indicated that the bolt holes in the bottom of the structure were significant in the model results, but the bolt holes in the top of the BA were insignificant. Finally, point masses equal to 0.42 g were placed at each of the nodes corresponding to the triaxial accelerometer locations. This significantly helped the model match experimental results as well.

Both the mass and stiffness matrices were then exported from Abaqus into MATLAB to have a greater control of the underlying information created by the model. This process required a reduction to make the matrices more easily handled in later calculations. The method used for this process was Guyan Reduction, which reduced the number of nodes by a factor of ∼225 while retaining much of the information about the dynamics. This reduction was verified by solving for the natural frequencies of the BA in MATLAB using the exported mass and stiffness matrices. These reduced results were then compared to the high-fidelity model, and were found to match closely with each other, having a mean average percent error of 0.34%.

A key requirement for testing and model validation was the proper selection of sensor and stinger locations such that the greatest number of modes would be excited. The sensor location was chosen using engineering judgement to obtain signal of a large enough magnitude that any noise might be overcome as well as avoiding symmetry which would generally result in redundant information. The location of the stingers and accelerometers can be seen in Figure 4.

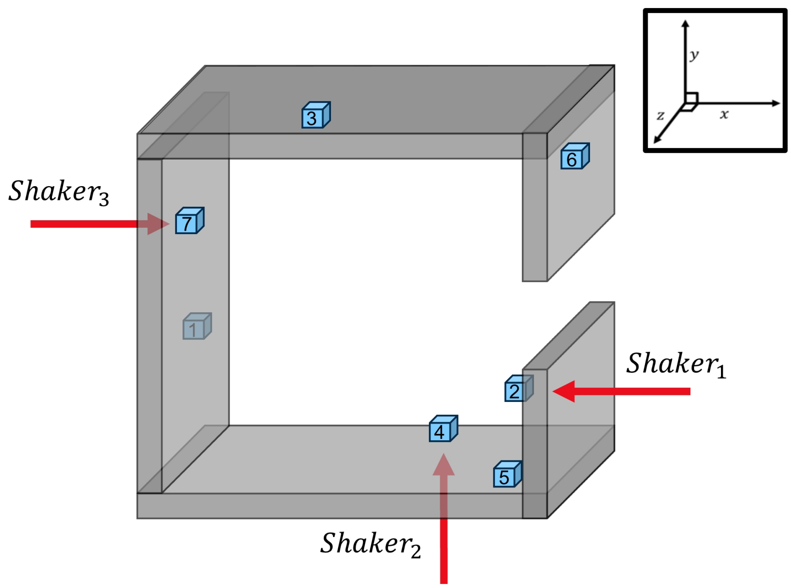

Fig. 4 Sensor and shaker placement for BA.

For the experimental setup, due to limited sensor availability as well as a limits on the number of channels from the Data Acquisition System (DAQ), a collection of six triaxial accelerometers, two load cells, and one uniaxial accelerometer were used to obtain all measurements. In order to excite the BA, three shakers were mounted to the structure seen in Figure 4 with stingers to minimize torsional loads. Since the DAQ had only two input channels, one shaker had to remain off for any specific testing scenarios. Even though only two shakers were used, keeping the third shaker attached was crucial to maintain consistent boundary conditions while switching between different testing scenarios seen in Figure 5.

Two of the triaxial accelerometers had a noisy z-direction, so those signals were neglected. The total number of individual signals that can be processed was nineteen. From the accelerometers, seventeen acceleration signals were obtained: seven signals in the x-direction, six signals in the y-direction, and four signals in the z-direction. The two active shakers each had load cells that were attached to the BA, which yielded two forcing signals.

For each test the two active shakers were given a burst random input signal to excite the BA. The burst random signal is preferable to randomly excite the BA with a span of 1-2000 Hz. Using a chirp input signal would have yielded similar results, but the burst random input signal was more time efficient, and no windowing was needed as long as our system's response decayed before the next burst.

There were six tests conducted in order to obtain the experimental data for both MIMO and SIMO systems; these setups can be seen in Figure 5. In the first MIMO test setup (MIMO 1), shaker one and shaker two excited the BA while shaker three remained off. The output of this stage yielded thirty-four FRFs, since there are two forcing locations and seventeen accelerometer channels. The second MIMO test setup (MIMO 2) had shaker two and shaker three exciting the BA while

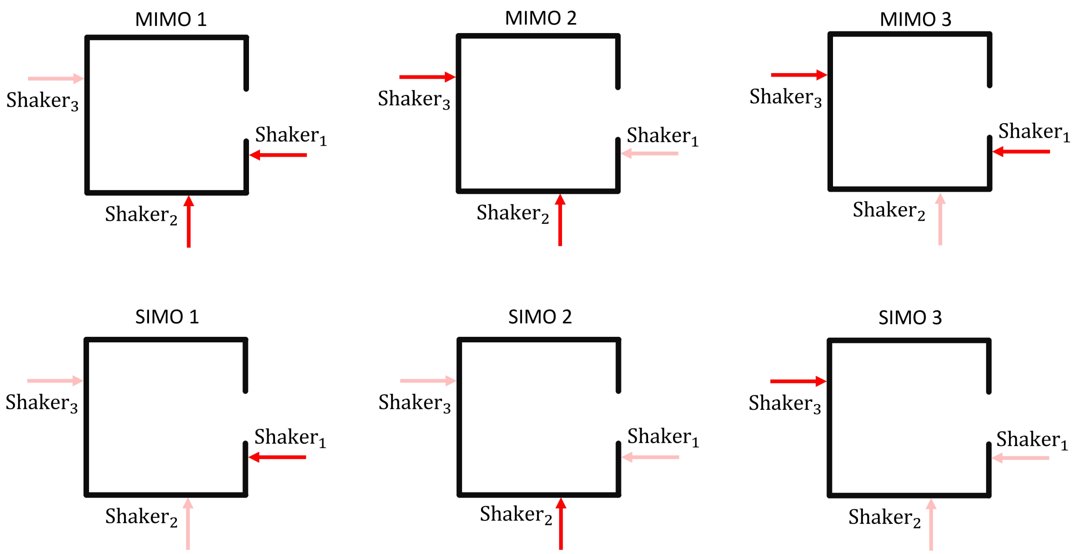

Fig. 5 The three MIMO and three SIMO experiments conducted.

shaker one remained off. The output of this stage yielded thirty-four FRFs with respect to forcing at shakers two and three. For the final MIMO test setup (MIMO 3), shakers one and three excited the BA while shaker two was off. The output of this stage yielded thirty-four FRFs with respect to forcing from shakers one and three. There were also three SIMO test setups following a similar pattern. In the first SIMO test setup (SIMO 1), shaker one excited the BA while shakers two and three were off. In the second test setup (SIMO 2), shaker two excited the BA while shakers one and three remained off. In the last SIMO test setup (SIMO 3), shaker three excited the BA while shakers one and two remained off. For each of the SIMO tests, 17 FRFs were created, with respect to forcing by the indicated shaker. Conclusions about differences in transfer paths between MIMO and SIMO systems can be drawn experimentally only with frequency ranges where the FRFs match. This indicates a similar system between setups, allowing for more accurate comparisons.

From these experiments the comparison between SIMO and MIMO FRFs have been made in Figure 6. These comparisons are necessary as they will help guide the conclusions of comparing the differences in transfer paths between MIMO and SIMO. In theory the FRFs from the MIMO and SIMO systems will be identical as long as the system and boundary conditions remain the same throughout each experiment. This means that all modes of the structure will excited and captured between different configurations. However, as displayed in Figure 6, the MIMO and SIMO FRFs do not match up exactly in some frequency ranges. It is important that no conclusions about the transfer paths are made based on the frequency ranges where the FRFs do not match. Since the SIMO experiments have only a single shaker receiving the burst random signal to excite the BA, some of the mode shapes can be misrepresented as the box assembly is unable to be fully excited from a single shaker. Conversely, the MIMO experiments have two active shakers exciting the box assembly. This allows for the system to be excited more equally across more modes, allowing better full system identification.

Clear deviations in Figure 6 for Shaker 1 and Shaker 3 Drive Points can be seen for MIMO3. For the MIMO3 setup, shakers 1 and 3 are driving, as seen in Figure 5. Where there is no excitation in the y-direction, and the excitation in the x-direction oppose each other, the response of the system changes slightly. This can also be seen for Shaker 2 Drive Point where the FRFs match each other much more closely up to about 600 Hz and no MIMO3 test occurs.

When evaluating the differences in transfer paths between SIMO and MIMO system experimentally, conclusions can only be made for regions where MIMO and SIMO FRFs are approximately equal. On the other hand, analytical FRFs are always equal regardless of the number of inputs.

As a result, this makes analyzing the difference in transfer paths easy as any conclusion made are valid for any frequency range. Figure 7 shows an 8-degree-of-freedom spring-mass linear system used in previous studies [1]. Evaluating the transfer paths for a SIMO system where the forcing is on mass one, the transfer paths can be obtained using Equation 10. Where $\{x_k\} = \{x_1\}$ and $\{x_u\} = \{x_5\}$. For the rest of the examples discussing different MIMO and SIMO systems, all of the transfer paths will follow Equation 10, while the only changes being made between the systems are forcing locations.

$$\{T\} = \{x_u\}\{x_k\}^{-1} = \{x_5\}\{x_1\}^{-1} = \{T_{51}\} \tag{10}$$

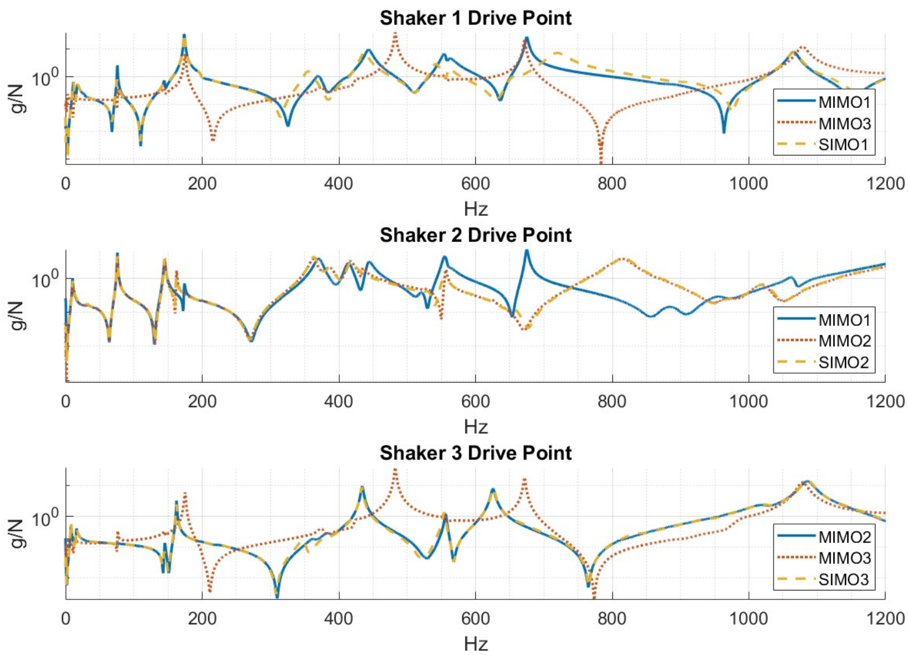

Fig. 6 Comparison of MIMO FRFs to SIMO FRFs with the same accelerometer to the same shaker.

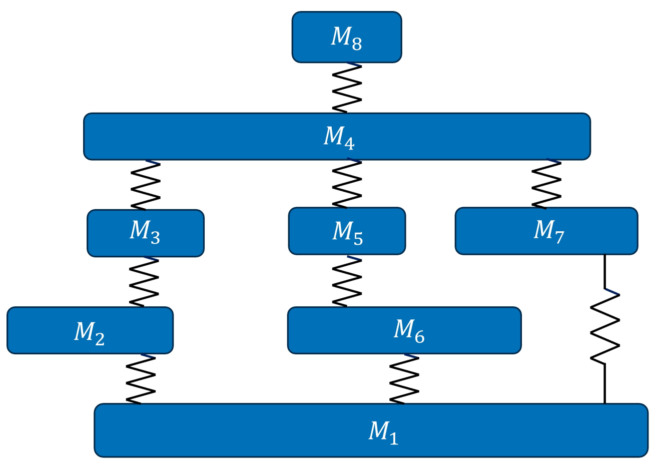

Fig. 7 Spring mass system used to evaluated transfer paths between MIMO and SIMO cases.

From the transfer path obtained from the SIMO case of forcing only on mass one, it is important to note that if the forcing on mass one is scaled up or down by some constant, the transfer path $\{T_{51}\}$ will not change. That is to say, the contribution of mass one to mass five will remain constant regardless of forcing magnitude. Which also means for a SIMO system where $\{x_k\}$ and $\{x_u\}$ are held constant, the transfer path will always be the same when forcing at a given location with any magnitude. For instance if $\{x_k\}$ and $\{x_u\}$ remain the same, then there could only be eight SIMO transfer paths obtained from individual forcing at all eight masses. For the analysis where $\{x_k\}$ and $\{x_u\}$ are kept constant, the eight transfer paths that can be obtained from the system in Figure 7 will be associated with each individual SIMO case.

When evaluating transfer paths for MIMO systems, it is important to note that the same rules for SIMO systems do not apply. Using the same $\{x_k\}$ and $\{x_u\}$, the transmissibility matrix can be obtained in a similar fashion to SIMO system. The difference is that there are now multiple forcing locations with different magnitudes. Here is where the MIMO transfer paths start to differ from the SIMO systems. If the transfer path $\{T_{51}\}$ is computed from forcing at multiple locations, then the transfer path will change depending on the magnitudes of the individual forcing. Letting the forcing magnitude be equal for each of the forcing locations, a balanced MIMO transfer path is obtained. As long as the forcing magnitudes are the same for any MIMO case and thus the magnitude ratio, $\{x_u\}/\{x_k\}$, is kept constant, then the balanced MIMO transfer paths will always be obtained. This can be a baseline for MIMO transfer paths as the balanced transfer paths reveal the responses from equal weighting from forcing at different locations. On the other hand, if forcing magnitudes start to differ from one location to another, then the transfer path obtained will start to diverge from the balanced MIMO transfer path. The resultant transfer path will then start to converge towards the SIMO transfer path corresponding to the force with the greatest magnitude in a MIMO system.

Let $\{x_k\}$ and $\{x_u\}$ remain the same from Equation 10 and have forcing on masses one, two, and three from Figure 7. The balanced transfer path $\{T_{51}\}$ can be obtained assuming $F_1 = F_2 = F_3$. Now three more transfer paths $\{T_{51}\}$ can be computed from the SIMO systems that make up the MIMO system. That is, $\{T_{51}\}$ forcing only on mass one, $\{T_{51}\}$ forcing only on mass two and $\{T_{51}\}$ forcing only on mass three. In Figure 8 the balanced transfer path $\{T_{51}\}$ obtained from the MIMO system is displayed, as well as the three SIMO transfer paths $\{T_{51}\}$ obtained from the three SIMO cases stated above. As stated previously, the balanced MIMO transfer path can be obtained only when multi-forcing magnitudes are equal. As forcing magnitudes deviate from each other, the MIMO transfer path will diverge from the balanced transfer path. In the limit where the relative forcing magnitude at one location exceeds the magnitude of forcing at other locations, the MIMO transfer path will start to converge towards the SIMO transfer path of the large forcing magnitude. This can also be shown in Figure 8, which shows the balanced transfer path $\{T_{51}\}$ obtained from the MIMO system stated above and the three SIMO convergences possibilities. As the forcing magnitude at one location exceeds the forcing magnitudes of the other locations, the figure shows the convergence of the MIMO balanced transfer path to a SIMO transfer path. This can also be reasoned out mathematically by recognizing that if one force was made large enough in Equation 11, the others would have increasingly little effect.

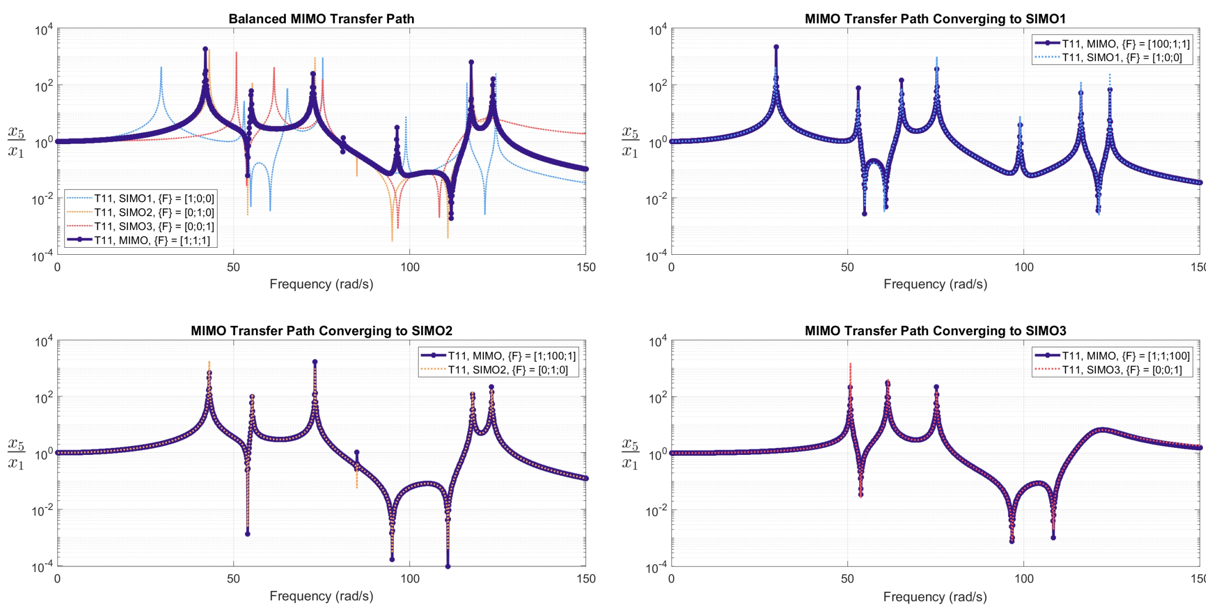

Fig. 8 MIMO transfer path converging to SIMO counterparts.

In other words, MIMO transfer paths are not complete linear combinations of the SIMO transfer paths as the relative multi forcing magnitude contributes significantly in computing the MIMO transfer path.

$$T_{12} = \frac{H_{11} \cdot F_1 + H_{12} \cdot F_2 + \cdots + H_{1n} \cdot F_n}{H_{21} \cdot F_1 + H_{22} \cdot F_2 + \cdots + H_{2n} \cdot F_n} \neq A \cdot \frac{H_{11} \cdot F_1}{H_{21} \cdot F_1} + B \cdot \frac{H_{12} \cdot F_2}{H_{22} \cdot F_2} + \cdots + X \cdot \frac{H_{1x} \cdot F_x}{H_{2x} \cdot F_x} \tag{11}$$

The correct calculation of transfer paths were key to the secondary goal, to predict the FRF between two unforced locations on the physical BA. Two methods for this goal were evaluated. The first approach that was attempted was the multiplication of a transfer path and an FRF to reach the desired transfer function. This operation can be seen in Equation 12, which relates frequency domain information and where subscript notation t is target, u is unknown and k is known.

$$\frac{X_t}{F_u} = \frac{X_t}{X_k} \cdot \frac{X_u}{F_k} \tag{12}$$

The FRF in this equation relating the force at the unknown point to the acceleration of the known point can be gathered without actually forcing at the unknown point by utilizing the concept of reciprocity of a linear structure and finding the FRF by forcing at the known point. Methods for gathering the transfer path have already been explored at length in this paper. Attempting this prediction method on the analytical spring mass system shown earlier results in Figure 9.

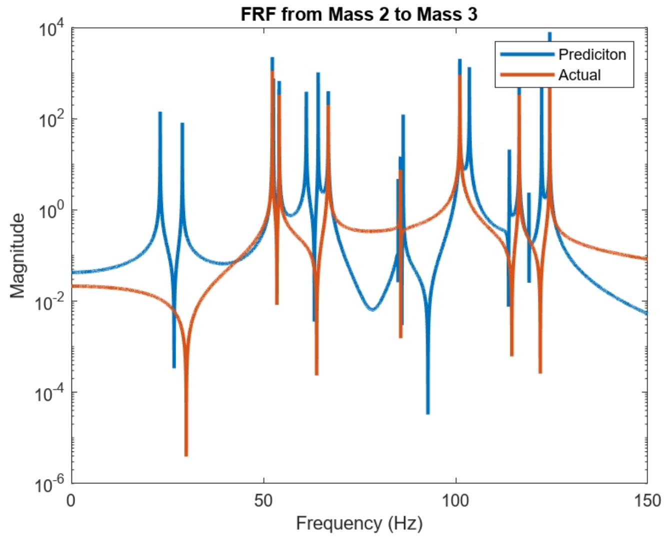

Fig. 9 FRF Prediction using Transfer Paths and FRFs

In an effort to improve the results of the prediction as well as to make it more applicable to the Box Assembly, numerical simulation data was used to predict the transfer paths which were then combined with experimental FRFs. The results of those calculations can be seen in Figure 10.

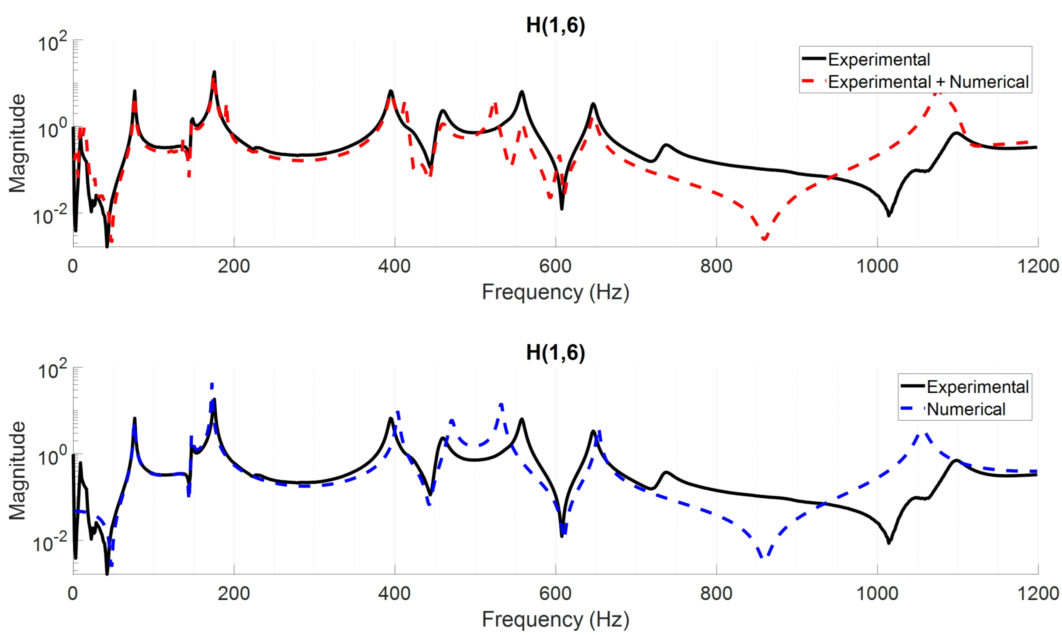

Fig. 10 Comparison of predictions of a mix of numerical and experimental data.

The second method used to predict the unknown FRF involved taking the matrix of FRFs gathered during a SIMO or MIMO test and retrieving modal parameters using the least squares rational function algorithm. The parameters that were retrieved were the mode shape matrix, the damping ratios for each mode, and the natural frequencies. Using these values, any FRF between two measured accelerometer locations could be predicted using Equations 13 and 14 as a template for the construction of FRFs where $[\Phi]$ is the mode shape matrix for an n-dof system with m-modes, and $[M]$ represents the inverse pole matrix. The results of our analysis built from Equation 13 are shown in figure 11 as our final conclusion for the predictability of these transfer functions.

$$[H] = [\Phi][M][\Phi]^T = \begin{bmatrix} \Phi_{11} & \Phi_{12} & \cdots & \Phi_{1m} \\ \Phi_{21} & \Phi_{22} & \cdots & \Phi_{2m} \\ \vdots & \vdots & \ddots & \vdots \\ \Phi_{n1} & \Phi_{n2} & \cdots & \Phi_{nm} \end{bmatrix} \begin{bmatrix} M_1 & 0 & \cdots & 0 \\ 0 & M_2 & \cdots & 0 \\ \vdots & \vdots & \ddots & \vdots \\ 0 & 0 & \cdots & M_x \end{bmatrix} \begin{bmatrix} \Phi_{11} & \Phi_{21} & \cdots & \Phi_{n1} \\ \Phi_{12} & \Phi_{22} & \cdots & \Phi_{n2} \\ \vdots & \vdots & \ddots & \vdots \\ \Phi_{1m} & \Phi_{2m} & \cdots & \Phi_{nm} \end{bmatrix} \tag{13}$$

$$M_x = \frac{-\omega^2}{\omega_{nx}^2 - \omega^2 + 2i\zeta_x\omega_{nx}\omega} \tag{14}$$

Conclusion

One of the key purposes of this paper was to investigate the differences between the transfer paths and transmissibility matrices of MIMO and SIMO systems. Towards this goal there were two main findings. The first was that as one of the forces applied in a MIMO system became an order of magnitude larger than any of the other forces, the transfer path between any two points converged to the path that would be seen in a SIMO case where just the larger force was present. The second key finding was that the MIMO transfer paths could not be constructed as a linear combination of SIMO cases.

In the effort to predict FRFs at locations that were never forced, the first method used measured transfer paths and FRFs in a calculation like Equation 12. This method did predict some peaks but was often vastly inaccurate. The error in this method was found to be in the assumption that the transfer path would be the same between the measured and predicted cases. This method necessitates a transfer path based on the frequency information from the unknown forcing case, however obtaining this data would be contrary to the original goal of not forcing at the location. Therefore, this method was unsuitable for experimental only prediction without the integration of some numerical simulation data.

The failure of the first method due to the inability to gather the needed transfer paths inspired an attempt to integrate numerical simulation predictions for transfer path into the calculation. The results of this method were seen in Figure 10. This method produced predictions that were improved from the prior method. However it was still erroneous, likely due to FE model inaccuracies used for numerical transfer path prediction or boundary condition differences between the model and the experiment. Another shortcoming of this method is that its requirement for highly accurate modeling makes solving for FRFs using simulation more reasonable than the method proposed.

The third attempt at FRF prediction followed roughly the method outlined in Equation 13. This method produced many of the best results as can be seen in Figure 11.

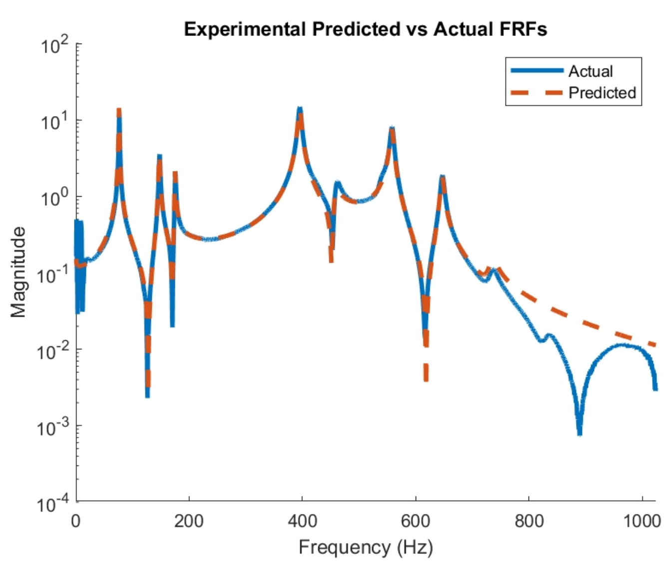

Fig. 11 Prediction of FRF from shaker 2 to accelerometer 7 from shaker 1 SIMO data.

This method provides good predictions for frequencies below 700 Hz, however there are some qualities that can improve its accuracy. The method of fitting the input FRFs can affect how well the overall system parameters can be gathered. It may also have some correlation to the quality of fitting the two accelerometer channels directly related to the desired FRF.

An analysis of the capabilities and limitations of this method for predicting FRFs as well as an analysis on what might improve these results is a topic deserving of further study. The benefits of a further refined and automated system for predictions would be well worth study as they would reduce time and cost for MIMO testing. This paper presents a novel approach for estimating the frequency response function at locations where only acceleration is measured. This method demonstrates reliability and accuracy up to approximately 700 Hz with our system. The methodology of estimating FRFs under these constraints offers a valuable tool to be used to reduce labor intensive experimentation.

Acknowledgments This research was funded by Los Alamos National Laboratory (LANL) through the Engineering Institute's Los Alamos Dynamics Summer School. The Engineering Institute is a research and education collaboration between LANL and the University of California San Diego's Jacobs School of Engineering. This collaboration seeks to promote multidisciplinary engineering research that develops and integrates advanced predictive modeling, novel sensing systems, and new developments in information technology to address LANL mission relevant problems.

References

1. N.M.M. Maia. J.M.M. Silva, A.R. "The transmissibility concept in multi-degree-of-freedom systems". *Mechanical Systems and Signal Processing*, 15:129–137 (2001)
2. António P.V. Urgueira, N.M.M., Raquel A.B. Almeida. "On the use of the transmissibility concept for the evaluation of frequency response functions". *Mechanical Systems and Signal Processing*, 25(3):940–951 (2011)
3. M. Fontul, J.S.N.M., A.M.R. Ribeiro. "Transmissibility matrix in harmonic and random processes". *Shock and Vibration*, 11:563–571 (2004)
4. Iván Gómez Araújo, J.E.L. "Operational modal analysis using svd of power spectral density transmissibility matrices". *Mechanical Systems and Signal Processing*, 46(1):129–145 (2014)
5. Leclère, Q., Roozen, N.B., and Sandier, C. "On the use of the hs estimator for the experimental assessment of transmissibility matrices". *Mechanical systems and signal processing*, 43(1-2):237–245 (2014)
6. X.Z. Li, X.D.Z.P., X.B. Yue. "Response transmissibility versus power spectrum density transmissibility: Dynamic property analysis and comparison". *Journal of Sound and Vibration*, 454:32–50 (2019)